

Exploring from *ab initio* calculations the structural and electronic properties of supported metal linear atomic chains on the NiAl (110) surface

Bruno Fedosse Zornio¹ · Edison Zacarias da Silva² · Miguel Angel San-Miguel¹

Received: 8 February 2017 / Accepted: 8 April 2017 / Published online: 21 April 2017
© Springer-Verlag Berlin Heidelberg 2017

Abstract Periodic density functional theory calculations were carried out to study the energetic and electronic properties of group 10 and 11 transition metal linear atomic chains (LACs) supported on the NiAl (110) surface. The only crystallographic direction that produces an effective LAC is with the metal atoms along the [001] direction. In other directions, the atoms adsorbed on stable adsorption sites are separated by large distances reducing the metal–metal interactions and consequently, preventing the formation of chemical bonding. The growth process of adding atoms, one by one, in the effective LACs is energetically favorable by increasing the number of metal atoms, for all tested transition metals. The Pt LACs experience the strongest interaction between the metals within the LAC and the weakest interaction between the LAC and the support resulting in an outstanding behavior with respect to the other transition metals.

Keywords NiAl · Adsorption · Linear atomic chain · DFT

Published as part of the special collection of articles derived from the 10th Congress on Electronic Structure: Principles and Applications (ESPA-2016).

Electronic supplementary material The online version of this article (doi:10.1007/s00214-017-2092-0) contains supplementary material, which is available to authorized users.

✉ Miguel Angel San-Miguel
smiguel@iqm.unicamp.br

Bruno Fedosse Zornio
bruno.zornio@iqm.unicamp.br

¹ Institute of Chemistry, University of Campinas, Unicamp, Campinas, SP 13083-970, Brazil

² Institute of Physics “Gleb Wataghin”, University of Campinas, Unicamp, Campinas, SP 13083-859, Brazil

1 Introduction

Within the scope of several challenges in the development of new nanomaterials nowadays, the understanding of how the system properties vary as function of material structure at atomic scale (size, dimensionality and aggregation) is a major goal [1]. However, the finest experimental techniques for nanomaterial characterization at atomic scale are very expensive, delicate and difficult.

From science and engineering applications points of view, the miniaturization of electronic devices can benefit from the development of controlled atomic wire systems [2], and for such systems the transport [3] and mechanical properties [4] must be controlled and understood. Atomic wires also exhibit distinct reactivity compared to the bulk [5], unveiling suitable chemical properties for catalysis applications.

More precisely, this article focuses on the computational modeling and characterization of a class of atomic wires obtained by Nilus et al. [6–11], which are based on atom-by-atom deposition of Au and Pd atoms over the (110) surface of NiAl alloy using STM (scanning tunneling microscopy) techniques. This fine and accurate method allows building supported atomic wires, so called linear atomic chains (LACs).

NiAl alloy is a unique material, and due to its light-weight and impressive mechanical and thermal resistances is widely used in the aerospace industry [12]. Furthermore, it has been used as useful convenient support for catalytic proposes [13]. The atomic structure consists of a bimetallic alloy with stoichiometric amount of Ni and Al atoms arranged in a bcc structure. The former works focusing on computational characterization and modeling of the properties of NiAl surfaces appeared in the late 80s [14–16].

The high stability of the (110) surface among all low index surfaces, and the strong affinity between substrate and adsorbates (metals in groups 10–11) cause the fundamental characteristics of a stable and well behaved system. Besides technology applications, it is an attractive system to modeling processes occurring on surfaces (e.g., molecular and atomic adsorption) [17–19]. Regarding specifically atomic wires supported on NiAl, some theoretical results exploring electronic, geometric and transport properties have already been reported for Au [20–22] and Pd [23]. These particular systems are also interesting from a fundamental point of view because there are some convenient experimental results to compare with.

Our research group has already been working on these systems, and in a first study [24], we investigated systematically the adsorption of metal transition adatoms from group 10 (Pd and Pt) and group 11 (Cu, Ag and Au) on the NiAl (110) surface. Later on, we analyzed the effect of increasing the surface coverage from 0.25 to 1.00 ML using a (2 × 2) surface cell model [25]. It was shown that for 0.5 ML the adatoms can be allocated along specific orientations, but forming linear atomic chains (LACs) only when oriented along the [001] crystallographic direction.

In this work, we extend our study using a larger (5 × 3) supercell allowing five adatoms to form the infinite LAC instead of only two as in the previous work. On doing so, we can investigate how the system evolves as the chain grows, starting from the monomer, and adding atoms, one by one, until reaching the infinite LAC. Another important characteristic in this larger system is that the bias due to the periodic conditions is alleviated and, consequently, this is a more realistic model.

2 Methodology

The present work is based on density functional theory (DFT), and all the calculations were performed with the Vienna ab initio Simulation Package (VASP) code [26, 27]. The valence electrons were described with a plane wave basis set using a kinetic energy cutoff of 270 eV, which was adequate to obtain total energy converged to at least 1 meV/atom. The projector augmented wave (PAW) method [28–30] was used to account for the effect of the electron core on the valence electron density. The electron exchange–correlation contribution was described using the generalized gradient approximation (GGA), specifically the Perdew–Wang (PW91) functional [31]. Methfessel–Paxton method with smearing width of 0.1 eV was used to integrate the Brillouin zone. The conjugated gradient (CG) algorithm was chosen for structural optimizations. Although NiAl is a nonmagnetic alloy, spin polarization calculations were performed for all cases.

The computational model used to simulate the LACs is based on the bcc NiAl bulk with lattice parameters of d_0 and $\sqrt{2} d_0$ for the (001) and (−110) directions, respectively. The d_0 parameter was computed in a previous work [24] using a 11 × 11 × 11 k -point grid resulting in a value of 2.91 Å in agreement with experimental data. All the geometry optimizations involved only the atoms keeping fixed the lattice parameters. The NiAl (110) surface was modeled on building a (3 × 5 × 4) slab with ~26 Å vacuum distance. This is a quite large supercell and the Monkhorst–Pack grid was set to 2 × 3 × 1 k -points for ionic optimizations although other finest grids were also tested, and no significant differences resulted in the energy system (<1 meV/atom). For electronic optimizations, a grid of 4 × 6 × 1 points was used in order to obtain more accurate results.

All plots of electronic charge differences ($\Delta\rho_{(xyz)}$) were generated with 0.0009 Bohr^{−3} iso-surfaces for all metal chains and different supercell orientations. The palette of colors varies from blue (negative) to red (positive), meaning depletion and accumulation electron density, respectively.

The STM images were produced based on the Tersoff and Hamann [32] methodology using the HIVE-STM program [33]. A bias voltage of −1.5 V was chosen. For each metal and template, the distance to the highest atom is different, and it was adjusted to attempt the best quality and homogeneity in the simulated STM images.

3 Results and discussion

3.1 LAC models and structure properties

The adsorption of transition metal adatoms has been studied previously, and seven potential adsorption sites were identified and analyzed. Furthermore, it was reported that the fourfold coordinated site (the adatom sits on Ni–Ni and Al–Al bridges) is the most favorable compared with other adsorption sites [6, 13, 17, 21, 24, 34]. These facts allow us to consider three different possibilities for the growth of linear atomic chains (LACs) on a (3 × 5) supercell of the NiAl (110) surface. Thus, we can locate atoms along three directions as illustrated in Fig. 1: three atoms on the diagonal (3D), three atoms along the [−110] direction (3L) and five atoms linearly positioned along the [001] direction (5L). Geometric optimizations for these three LAC models were carried out for LACs made of Pd, Pt, Cu, Ag and Au. The stability of the resulting systems can be analyzed from useful energy contributions as follows:

$$E_b = \frac{E_{\text{tot}} - E_{\text{surf}} - N_{\text{at}}E_{\text{at}}}{N_{\text{at}}} \equiv E_{M-S} + E_{M-M} \quad (1)$$

where E_b is the total binding energy per atom for each LAC model; E_{tot} is the total energy of the relaxed adsorption

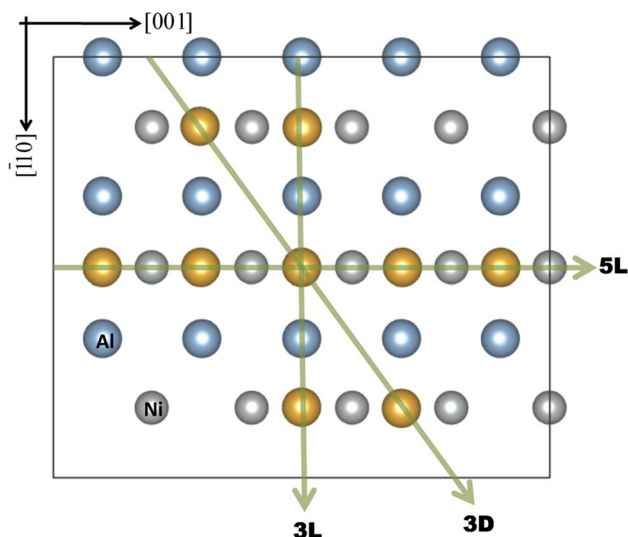


Fig. 1 Top view of the (3×5) supercell representing the NiAl (110) surface. Atoms are displayed as spheres (Ni in gray, Al in blue and adatoms in gold). The green arrows indicate 3D, 3L and 5L LAC models. The black arrows in the superior left corner point out specific lattice directions

system; E_{surf} is the isolated slab energy and $N_{\text{at}} * E_{\text{at}}$ is the adsorbate energy (N_{at} is the number of adsorbed atoms and E_{at} is the energy of the isolated adatom in the ground electronic state).

The binding energy can also be estimated from the last term in Eq. 1 where $E_{\text{M-S}}$ (Eq. 2) is the interaction energy between the atomic chain and the substrate; and $E_{\text{M-M}}$ (Eq. 3) accounts for the interaction energy between the chain metal atoms. Now, E_{adats} is the total energy of the LAC at the vacuum keeping the structure from adsorption.

$$E_{\text{M-S}} = \frac{E_{\text{tot}} - E_{\text{surf}} - E_{\text{adats}}}{N_{\text{at}}} \quad (2)$$

$$E_{\text{M-M}} = \frac{E_{\text{adats}} - N_{\text{at}}E_{\text{at}}}{N_{\text{at}}} \quad (3)$$

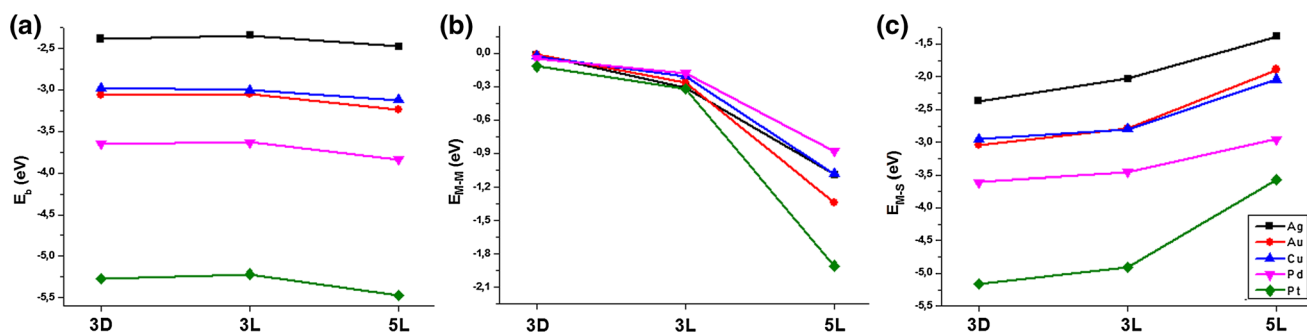


Fig. 2 a Total binding energy, E_b ; b metal–metal interaction energy in the chain, $E_{\text{M-M}}$; and c metal–surface interaction energy, $E_{\text{M-S}}$, for each metal in the three LAC models

The plots in Fig. 2 show all these three energy components as a function of the LAC model for all metal LACs. More precisely, Fig. 2a depicts the total binding energy which is almost constant, independently of the LAC model used, and the energy decreases in the following order: $\text{Ag} > \text{Au} > \text{Cu} > \text{Pd} > \text{Pt}$. This trend agrees with previous results [24, 25] for the study of adsorption of atomic monomers on the NiAl (110) surface. On the other hand, the energy components $E_{\text{M-S}}$ and $E_{\text{M-M}}$ in Fig. 2b, c, exhibit clear dependence as function of the metal considered. On comparing the proposed LACs models, for 3D and 3L systems, $|E_{\text{M-M}}| \ll |E_{\text{M-S}}|$, implying that the major contribution to E_b is the $E_{\text{M-S}}$ energy component. On the contrary, for the 5L LAC model, $E_{\text{M-M}}$ plays a significant contribution on E_b .

On relating structural results from Table 1 with the energies in Fig. 2, it is possible to observe that the distances between the adatoms are longer for 3L and 3D models; and $E_{\text{M-M}}$ (Fig. 2b) is almost negligible for 3D and very weak for 3L. This means that the stabilization energy is mainly due to the $E_{\text{M-S}}$ component indicating a strong coupling between the adsorbates and the substrate. On the other hand, for 5L model, both shorter distances (Table 1) and more negative $E_{\text{M-M}}$ values (Fig. 2b) suggest a strong coupling along the atoms within the chain. Consequently, it is possible to argue that only the 5L model is compatible with the formation of an effective LAC.

In order to better understand the energetics of the chain growth process, the E_b , $E_{\text{M-M}}$ and $E_{\text{M-S}}$ values were also computed for the smaller structures (dimer, trimer

Table 1 Mean distance (\AA) between the metal atoms for each one LAC model

	$d_{\text{Ag/Ag}}$	$d_{\text{Au/Au}}$	$d_{\text{Cu/Cu}}$	$d_{\text{Pd/Pd}}$	$d_{\text{Pt/Pt}}$
3D	5.08	5.08	5.06	5.09	5.08
3L	4.10	4.10	4.10	4.10	4.10
5L	2.91	2.92	2.92	2.92	2.92

and tetramer) on the NiAl (110) surface along the [001] direction (Fig. 3). It can be observed that the total binding energy E_b as a function of the chain length (Fig. 3a) is almost constant with a slight energy decline when the LAC is formed. This behavior (more pronounced for Pt) might be related to the fact that the LACs exhibit a structure with higher stability than the shorter analogous structures (2, 3 and 4 atoms). Another important feature observed from Fig. 3b, c is that E_{M-M} decreases as E_{M-S} increases (in order to keep E_b constant) when the chain develops. This behavior indicates that the interaction between the atoms within the chains increases as the chain length grows. For group 10 metals, there is a remarkable stabilization in E_{M-M} from dimer to trimer, whereas for group 11, the E_{M-M} is almost constant when the chain length enlarges.

The gain (or loss) in the energy stabilization as function of the chain length was estimated from the growth energy (E_G). E_G (Eq. 4) is defined as the difference between the total binding energy (E_b) and the adsorption energy of the

monomer in the fourfold coordination site (E_{mon}). It represents the energy cost for the chain building. If the value is positive, it means that the process of adding an atom has an energetic cost. On contrary, if E_G is negative, the process is energetically favorable.

$$E_G = E_b - N_{\text{at}}E_{\text{mon}} \quad (4)$$

From Fig. 3d it is possible to compare E_G for each metal atom and chain length. A general trend is that E_G decreases as the chain grows. More precisely, two main features must be highlighted: the first one is the significant energy change $\Delta E_{G(1 \rightarrow 2)}$ from monomer to dimer; and the second one is another stabilization $\Delta E_{G(4 \rightarrow 5)}$ when reaching the LAC formation (Fig. 4).

3.2 Electronic properties

In order to further understand the electronic properties of the supported LACs on the NiAl (110) surface, it was

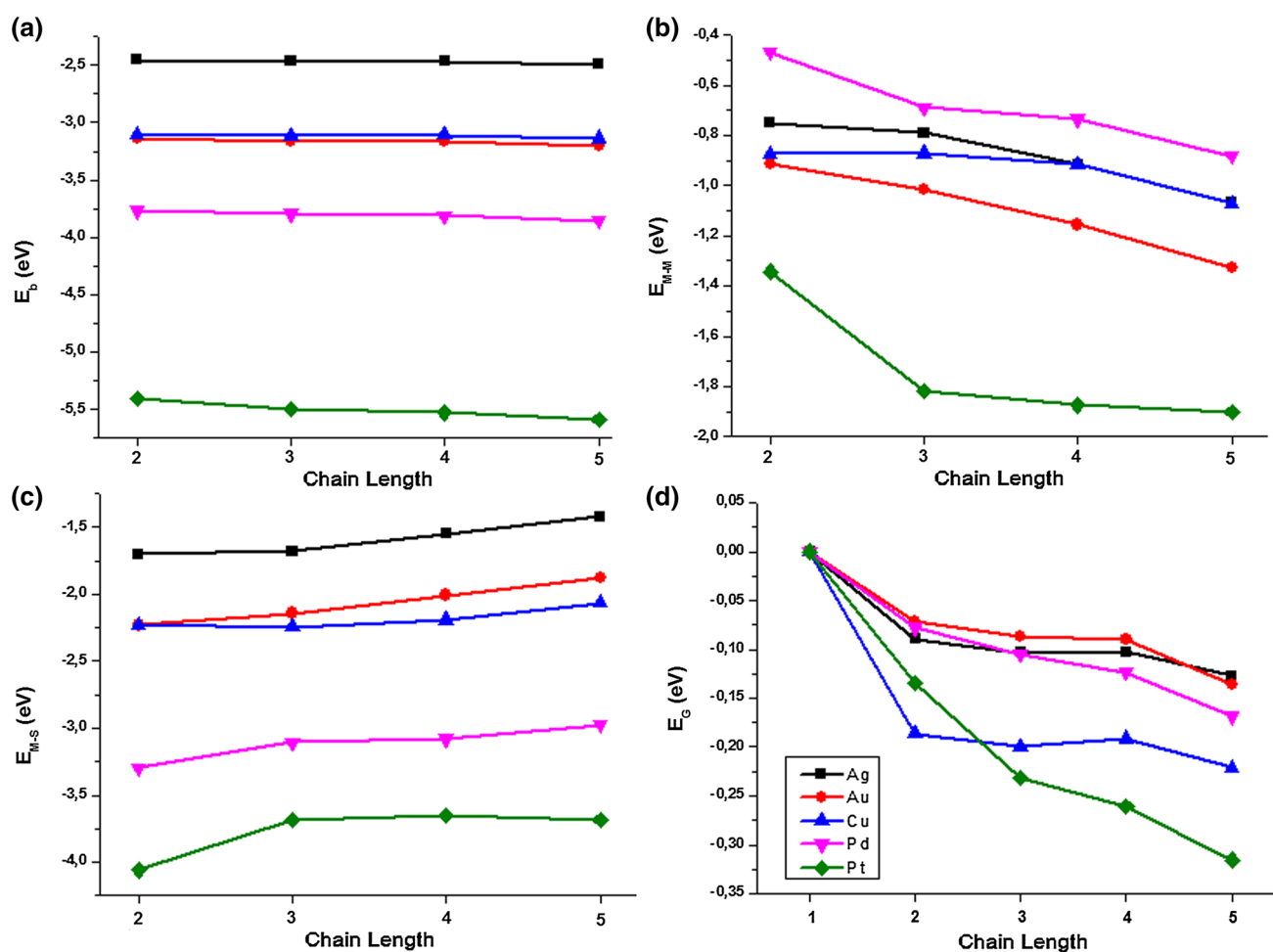


Fig. 3 **a** Total binding energy, E_b ; **b** metal-metal interaction energy in the chain, E_{M-M} ; and **c** metal-surface interaction energy, E_{M-S} , **d** growth energy, E_G , as a function of the chain length

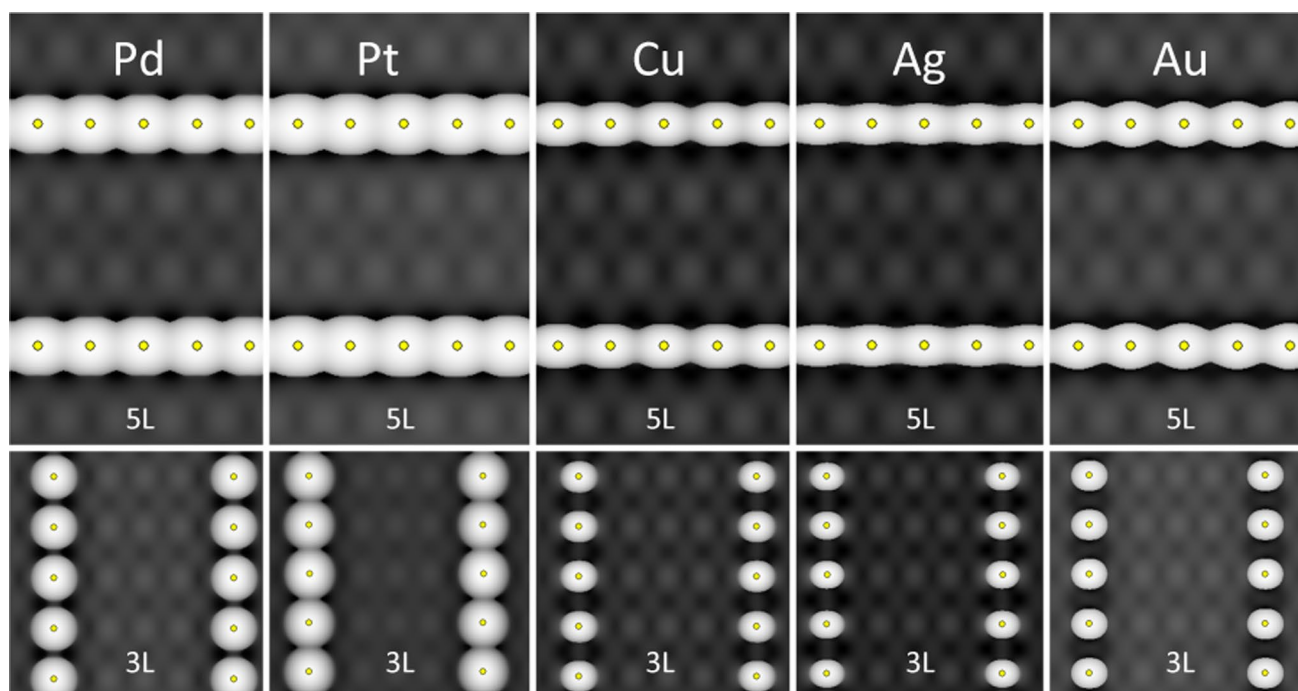


Fig. 4 Simulated STM images generated using the Tersoff–Hamann method for the 5L and 3L LAC models using a voltage bias of -1.5 V

useful to simulate STM (scanning electron microscopy) images using the Tersoff and Hamann [32] method. The yellow small circle in Fig. 4 indicates the position of the adsorbed atom. The topology of the surface is in gray scale

(white means highest position and black deepest position). It becomes apparent that all the 5L models show a strong binding between the adatoms proving the formation of LACs. In contrast, the 3L models exhibit a typical behavior

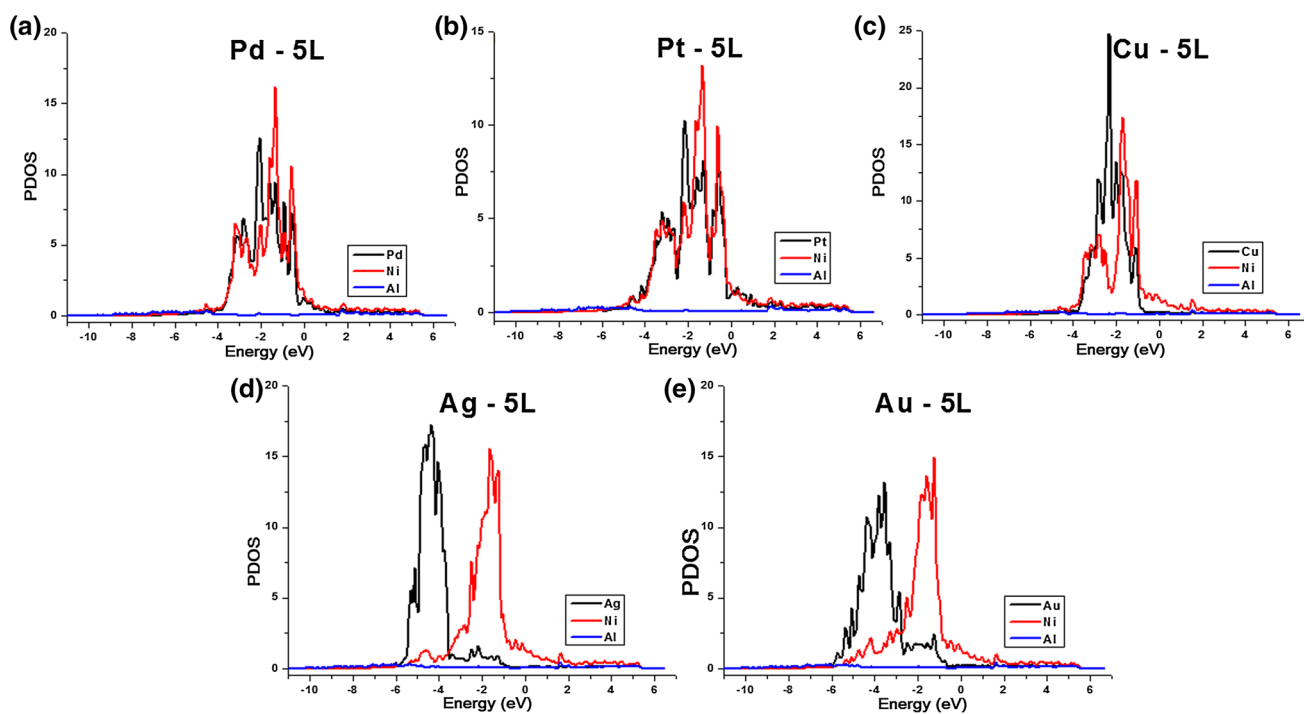


Fig. 5 Projected local density of states (PDOS) for each metal in the 5L LAC model

of isolated adatoms except for Pt, in which a slight contact can be observed.

The electronic structure was also studied from the analysis of the density of states (DOS) in order to shed light into the nature of the chemical bonding in the 5L models. Precisely, the projected density of states (PDOS) along d states for adatom (black line) and the nearest surface Ni (red line) and Al (green line) atoms are plotted in Fig. 5. The s and p projections are omitted due to their very low contribution.

It can be observed from the PDOS plots in Fig. 5 important differences for group 10 (Pd and Pt) and group 11 (Cu, Ag and Au). First, the occupied electronic states for both Pd and Pt (Fig. 5a, b) are in the same energy range than the surface Ni electronic states (-3 eV to 0 eV), moreover, all the states with the higher population (the prominent peaks in the PDOS plots) are coincident for Ni and group 10 metal chains. Based on these two observations, it is possible to conclude that there is a strong coupling across the electronic states indicating a significant covalent metallic character between the chain atoms and the surface Ni atoms [25, 17]. Secondly, for group 11 metals, especially for Ag and Au (Fig. 5d, e), there is virtually no electronic states superposition between adsorbate and substrate. This fact is characteristic of an electrostatic interaction as it will be reviewed below. Differently, Cu exhibits a singular behavior, being more similar to group 10 metals, with the d band also coincident with the Ni d band, and possibly revealing an intermediate behavior between the two groups.

It is worth noticing that the PDOS for the chain atoms show different behavior according to the LAC model (black line in Fig. 5). Thus, in 3L and 3D models with metal atoms separated by larger distances (see Supplementary

Material), Ag and Au exhibit sharp distributions, while for the real LAC system (5L model), the PDOS is clearly broader, suggesting that the bond character along the chain atoms is covalent metallic. This assertion is also claimed in other works from the literature [17, 24, 21].

The analysis of the electron charge differences is a very well established and useful tool in DFT studies when studying adsorption processes on solid substrates and it has been used successfully in other works related to adsorption NiAl (110) systems [15–17, 21, 23, 24]. This analysis provides information on how the electron density is redistributed after the interaction between the adsorbates and the substrate and may provide important information about the bonding formation.

In this work, the electron charge differences $\Delta\rho_{(xyz)}$ were calculated in all spatial coordinates, similar to what have been done to calculate E_b , (however, ρ is a matrix instead of a scalar.). The charge density of the isolated surface $\rho_{\text{surf}(xyz)}$ and the isolated chain $\rho_{\text{adats}(xyz)}$ are subtracted from the charge density of the total adsorption system $\rho_{\text{tot}(xyz)}$ (Eq. 5). During the bonding formation, the electron density is pulled out from the blue zones (negative $\Delta\rho$) to fill the yellow zones (positive $\Delta\rho$).

$$\Delta\rho_{(xyz)} = \rho_{\text{tot}(xyz)} - \rho_{\text{surf}(xyz)} - \rho_{\text{adats}(xyz)} \quad (5)$$

There are some general features observed from the iso-surfaces for LAC systems in Fig. 6. First, there is a clear depletion of the charge density (blue) meaning that the electron density was withdrawn from Al adsorbates (see the ‘bottom’, ‘side (001)’ and ‘cut (-110)’ views). In other words, this fact suggests an ionic character binding between the adsorbates and the surface Al atoms. Other

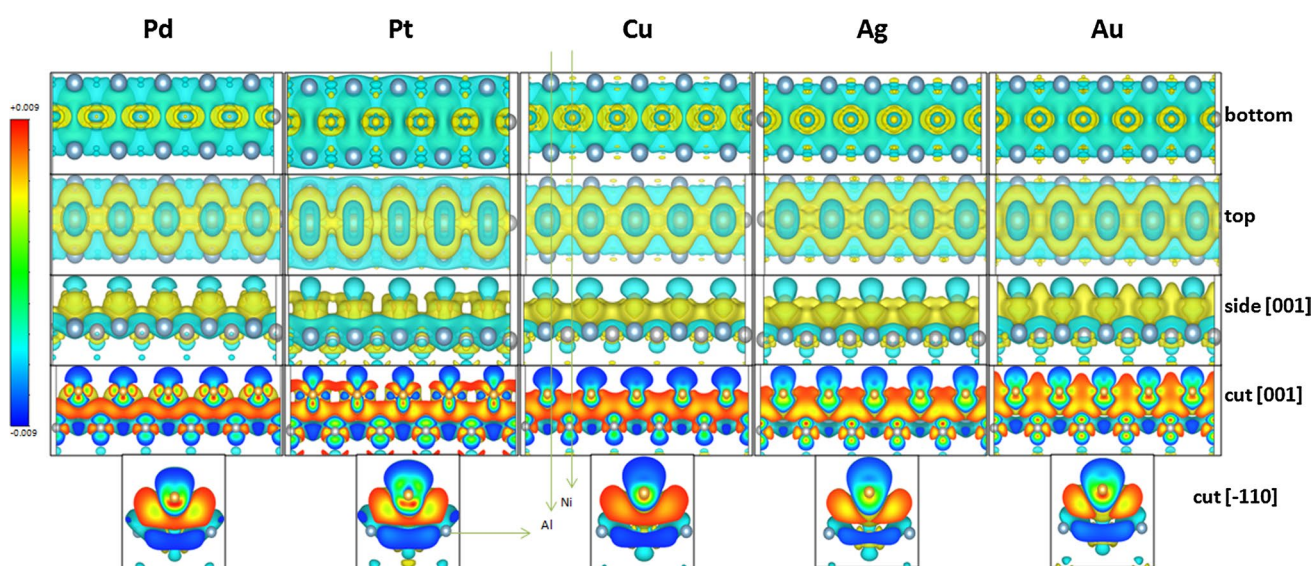


Fig. 6 Iso-surfaces of electron charge differences in different views for each metal in the 5L LAC model

important feature is related to the covalent metallic bond character with the closer surface Ni atoms (it can clearly be seen in the ‘top’ and ‘cut (001)’ views), the electron density shape suggests a d bond type. Both analyses are also corroborated with the previous PDOS discussion. The lateral interactions between the chain atoms become apparent when looking at the electron density accumulating between the chain atoms.

Furthermore, the ‘cut (001)’ and ‘cut (−110)’ images from Fig. 6 suggest that the adatom withdraws electronic charge from the surface. More accurate analysis shows significant charge accumulation around the chain atom (for all systems) and less meaningful around Ni atoms, meanwhile there is charge depletion around Al atoms. As a matter of fact, although the Ni electronegativity is comparable with Ag and Cu, all the metals in that series have a higher electronegativity than Ni (either with Al), resulting in a charge accumulation on the supported chain, and a charge deficiency in the surface.

4 Conclusions

First principles calculations based on periodic DFT have been carried out to gain insight into the structural, energetic and electronic structure of linear atomic chains grown on the NiAl (110) surface. Differently from our previous studies, we have made use of a large (5×3) supercell allowing allocation of 3 or 5 atoms along the three different surface directions.

The electronic analysis from simulation of STM images demonstrates that a real LAC is formed only when the adatoms are placed along the [001] direction. The decomposition of the binding energy into metal–metal and metal–surface contributions was useful to verify that the interaction between the adatoms is negligible for the 3D and 3L models, being quite significant for the 5L model.

In particular, the Pt LAC shows an intriguing behavior with respect to the other transition metals because the interaction between the metals within the LAC is the strongest, and the interaction between the LAC and the support is the weakest. This fact might involve singular conductance properties in the fabrication of LACs as wires in nanodevices.

The analysis of the projected local density of states (PDOS) and electron charge differences indicate that the chemical bonding between the LAC and the substrate is mainly covalent metallic for group 10 metals involving strong d orbital coupling between the LAC atoms and surface Ni atoms, meanwhile for group 11 metals the ionic interaction with surface Al atoms is more significant, except for Cu, which shows an intermediate behavior. On the other hand, the interaction between metals within the LAC is mainly contributed by d orbital coupling.

Acknowledgements The simulations were performed at the National Center for High Performance Computing in São Paulo (CENA-PAD) and at the CCJDR-UNICAMP. We acknowledge support from FAPESP (2013/07296-2, 2015/19709-5 projects). EZdS acknowledges support from CNPq (Grant 304073/2015-6) and BFZ thanks to CNPq for the Ph.D. Grant.

References

- Alivisatos AP (1996) Semiconductor clusters, nanocrystals, and quantum dots. *Science* 271:933–937. doi:[10.1126/science.271.5251.933](https://doi.org/10.1126/science.271.5251.933)
- Yanson AI, Bollinger GR, van den Brom HE et al (1998) Formation and manipulation of a metallic wire of single gold atoms. *Nature* 395:783–785. doi:[10.1038/27405](https://doi.org/10.1038/27405)
- Ohnishi H, Kondo Y, Takayanagi K (1998) Quantized conductance through individual rows of suspended gold atoms. *Nature* 395:780–783. doi:[10.1038/27399](https://doi.org/10.1038/27399)
- Rubio-Bollinger G, Bahn SR, Agraït N et al (2001) Mechanical properties and formation mechanisms of a wire of single gold atoms. *Phys Rev Lett* 87:26101. doi:[10.1103/PhysRevLett.87.026101](https://doi.org/10.1103/PhysRevLett.87.026101)
- Nascimento APF, San-Miguel MA, Da Silva EZ (2014) Unveiling the origin of oxygen atomic impurities in Au nanowires. *Phys Rev B Condens Matter Mater Phys* 89:1–6. doi:[10.1103/PhysRevB.89.085417](https://doi.org/10.1103/PhysRevB.89.085417)
- Nilius N, Wallis TM, Ho W (2002) Development of one-dimensional band structure in artificial gold chains. *Science* 297:1853–1856. doi:[10.1126/science.1075242](https://doi.org/10.1126/science.1075242)
- Nilius N, Wallis TM, Ho W (2002) Electronic density oscillations in gold atomic chains assembled atom by atom. *Phys Rev Lett* 89:236802. doi:[10.1103/PhysRevLett.89.236802](https://doi.org/10.1103/PhysRevLett.89.236802)
- Nilius N, Wallis TM, Persson M, Ho W (2003) Distance dependence of the interaction between single atoms: gold dimers on NiAl (110). *Phys Rev Lett* 90:196103. doi:[10.1103/PhysRevLett.90.196103](https://doi.org/10.1103/PhysRevLett.90.196103)
- Nilius N, Wallis TM, Ho W (2004) Building alloys from single atoms: Au–Pd chains on NiAl (110). *J Phys Chem B* 108:14616–14619. doi:[10.1021/jp049127r](https://doi.org/10.1021/jp049127r)
- Nilius N, Wallis TM, Ho W (2005) Tailoring electronic properties of atomic chains assembled by STM. *Appl Phys A Mater Sci Process* 80:951–956. doi:[10.1007/s00339-004-3121-0](https://doi.org/10.1007/s00339-004-3121-0)
- Nilius N, Wallis TM, Ho W (2005) Realization of a particle-in-a-box: electron in an atomic Pd chain. *J Phys Chem B* 109:20657–20660. doi:[10.1021/jp053496l](https://doi.org/10.1021/jp053496l)
- Darolia R (1991) NiAl alloys for high temperature structural applications. *JOM* 43:44–48. doi:[10.1007/BF03220163](https://doi.org/10.1007/BF03220163)
- Hanbicki AT, Scheffler M (1995) The interaction of hydrogen with the (110) surface of NiAl. *Surf Sci* 333:811–817. doi:[10.1016/0039-6028\(95\)00376-2](https://doi.org/10.1016/0039-6028(95)00376-2)
- Davis HL, Noonan JR (1985) Rippled relaxation in the (110) surface of the ordered metallic alloy NiAl. *Phys Rev Lett* 54:566–569. doi:[10.1103/PhysRevLett.54.566](https://doi.org/10.1103/PhysRevLett.54.566)
- Kang MH, Mele EJ (1987) NiAl(110) surface: First-principles determination of the rippled relaxation. *Phys Rev B* 36:7371–7377. doi:[10.1103/PhysRevB.36.7371](https://doi.org/10.1103/PhysRevB.36.7371)
- Lee JI, Fu CL, Freeman J (1987) All-electron local-density theory of the rippled NiAl (110) surface. *Phys Rev B* 36:9318–9321. doi:[10.1103/PhysRevB.36.9318](https://doi.org/10.1103/PhysRevB.36.9318)
- Carling KM, Glover W, Gunaydin H et al (2006) Comparison of S, Pt, and Hf adsorption on NiAl (110). *Surf Sci* 600:2079–2090. doi:[10.1016/j.susc.2006.02.047](https://doi.org/10.1016/j.susc.2006.02.047)

18. Borck Ø, Svenum IH, Borg A (2009) Adsorption of methanol and methoxy on NiAl (110) and Ni₃Al (111): a DFT study. *Surf Sci* 603:2378–2386. doi:[10.1016/j.susc.2009.05.034](https://doi.org/10.1016/j.susc.2009.05.034)
19. Evecen M, Çakmak M (2010) Adsorption of S, O, and H on the NiAl (110)-(2 × 2) surface. *Phys B Condens Matter* 405:4059–4063. doi:[10.1016/j.physb.2010.06.056](https://doi.org/10.1016/j.physb.2010.06.056)
20. Persson M (2004) Computational study of electron states in Au chains on NiAl (110). *Phys Rev B Condens Matter Mater Phys* 70:1–9. doi:[10.1103/PhysRevB.70.205420](https://doi.org/10.1103/PhysRevB.70.205420)
21. Calzolari A, Nardelli MB (2005) First principles theory of artificial metal chains on NiAl (110) surface. *Phys Rev B Condens Matter Mater Phys* 72:1–9. doi:[10.1103/PhysRevB.72.045416](https://doi.org/10.1103/PhysRevB.72.045416)
22. Calzolari A, Cavazzoni C, Nardelli MB (2004) Electronic and transport properties of artificial gold chains. *Phys Rev Lett* 93:7–10. doi:[10.1103/PhysRevLett.93.096404](https://doi.org/10.1103/PhysRevLett.93.096404)
23. Wu P, Yin N, Cheng W et al (2016) Structure and electronic properties of palladium chains supported by NiAl (110): a first-principles study. *Comput Mater Sci* 124:398–402. doi:[10.1016/j.commatsci.2016.08.008](https://doi.org/10.1016/j.commatsci.2016.08.008)
24. San-Miguel MA, Amorim EPM, da Silva EZ (2013) Adsorption of Pd, Pt, Cu, Ag, and Au monomers on NiAl (110) surface: a comparative study from DFT calculations. *J Phys Chem A* 118:5748–5755. doi:[10.1021/jp405877k](https://doi.org/10.1021/jp405877k)
25. San-Miguel MA, Amorim EPM, da Silva EZ (2015) NiAl (110) surface as a template for growing transition metal linear atomic chains: a DFT investigation. *J Phys Chem C* 119:2456–2461. doi:[10.1021/jp5097635](https://doi.org/10.1021/jp5097635)
26. Kresse G, Furthmüller J (1996) Efficiency of ab initio total energy calculations for metals and semiconductors using a plane-wave basis set. *Comput Mater Sci* 6:15–50. doi:[10.1016/0927-0256\(96\)00008-0](https://doi.org/10.1016/0927-0256(96)00008-0)
27. Kresse G, Furthmüller J (1996) Efficient iterative schemes for ab initio total-energy calculations using a plane-wave basis set. *Phys Rev B* 54:11169–11186. doi:[10.1103/PhysRevB.54.11169](https://doi.org/10.1103/PhysRevB.54.11169)
28. Payne MC, Teter MP, Allan DC et al (1992) Iterative minimization techniques for ab initio total-energy calculations: molecular dynamics and conjugate gradients. *Rev Mod Phys* 64:1045–1097. doi:[10.1103/RevModPhys.64.1045](https://doi.org/10.1103/RevModPhys.64.1045)
29. Blöchl PE (1994) Projector augmented-wave method. *Phys Rev B* 50:17953–17979. doi:[10.1103/PhysRevB.50.17953](https://doi.org/10.1103/PhysRevB.50.17953)
30. Kresse G (1999) From ultrasoft pseudopotentials to the projector augmented-wave method. *Phys Rev B* 59:1758–1775. doi:[10.1103/PhysRevB.59.1758](https://doi.org/10.1103/PhysRevB.59.1758)
31. Perdew J, Chevary J, Vosko S et al (1993) Erratum: atoms, molecules, solids, and surfaces: Applications of the generalized gradient approximation for exchange and correlation. *Phys Rev B* 48:4978. doi:[10.1103/PhysRevB.48.4978.2](https://doi.org/10.1103/PhysRevB.48.4978.2)
32. Tersoff J, Hamann D (1983) Theory and application for the scanning tunneling microscope. *Phys Rev Lett* 50:1998–2001. doi:[10.1103/PhysRevLett.50](https://doi.org/10.1103/PhysRevLett.50)
33. Vanpoucke DEP, Brocks G (2008) Formation of Pt-induced Ge atomic nanowires on Pt/Ge (001): a density functional theory study. *Phys Rev B* 77(241308):1–4. doi:[10.1103/PhysRevB.77.241308](https://doi.org/10.1103/PhysRevB.77.241308)
34. Wu P, Cao G, Tang F, Huang M (2013) First-principles study of small palladium clusters on NiAl (110) alloy surface. *Physica E* 53:7–13. doi:[10.1016/j.physe.2013.04.013](https://doi.org/10.1016/j.physe.2013.04.013)